# High strength fiber reinforced one-part alkali activated slag/fly ash binders with ceramic aggregates: Microscopic analysis, mechanical properties, drying shrinkage, and freeze-thaw resistance

Z. Abdollahnejad [a,*], M. Mastali [b], B. Woof [c], M. Illikainen [b]

[a] Civil & Environmental Engineering Department, University of Connecticut, 261 Glenbrook Road Unit 3037, Storrs, CT 06269-3037, USA
[b] Fibre and Particle Engineering Research Unit, University of Oulu, Pentti Kaiteran katu 1, 90014 Oulu, Finland
[c] Department of Chemical Engineering, Loughborough University, Leicester LE11 3TZ, Leicestershire, UK

## ARTICLE INFO

## ABSTRACT

One-part alkali-activated binders, also known as the "just-add-water" concept, have received great attention due to their advantages over two-part alkali-activated binders. By avoiding the use of dangerous alkali solutions, these binders are easier to both handle and transport. Ground granulated blast furnace slag is one of the side streams, which can be used in one-part alkali-activated binders to reach high compressive strength at an early age. However, using slag alone has some disadvantages, including a fast setting time and a large drying shrinkage, narrowing the application of these mix compositions and causing crack formation, respectively, thus shortening service life. Fly ash can be used in one-part alkali-activated materials to partially substitute for slag in order to both minimize drying shrinkage and prolong the setting time. Moreover, ceramic waste can be used as a replacement for normal sand, which is great achievement in terms of developing environmentally friendly alkali-activated materials exclusively from side steam. This paper presents new research on the effects on the fresh and hardened-state properties of one-part alkali-activated mortars of replacing up to 80% of slag with fly ash. These properties were characterized by the initial and final setting time, the strength development (compressive and flexural), and the drying shrinkage. Microstructural analyses (SEM/EDS, XRF, TGA/DTG) justified the results. Moreover, different fiber contents and combinations were used to reinforce the developed one-part alkali-activated slag/fly ash mortars to increase the strength, further reduce the drying shrinkage, and improve the freeze/thaw resistance. The results showed that fly ash and fibers can reduce the drying shrinkage and prolong the setting time. The weakened mechanical properties caused by decreasing the amount of slag are still adequate to let the composite slag/fly ash material be considered in construction applications.

© 2020

## 1. Introduction

Concrete is a common construction material that has traditionally relied on ordinary Portland cement (OPC) as a binder, along with aggregate and water. The production of OPC releases significant $CO_2$ emissions, however, composing approximately 8% of total global, human-caused $CO_2$ emissions [1]. In the OPC manufacturing process, the de-carbonation reaction of limestone at extreme temperatures (1400–1500 °C) is the major cause (50–60%) of the $CO_2$ emissions [2]. Alkali-activated binders as alternative materials with lower $CO_2$ emissions have been proposed to maximize the use of waste/recyclable material to produce construction products [3–5]. Alkali-activated binders react differently than OPC to the incorporation of various raw materials. In general, there are two main kinds of alkali-activated binders: 1)

more common, two-part alkali-activated binders, which are comprised of liquid alkali solutions and have harsh properties, like corrosiveness, high viscosity, and difficulty of on-site use [2]; and 2) one-part alkali-activated binders, which only require water to be added to the binder–alkali activator mixture in its solid shape. One-part alkali-activated binders have various advantages over traditional, two-part alkali-activated binders, such as being safe and easy to use. This makes one-part alkali-activated binders a good option for both on-site casting and commercial use in construction applications [6].

In alkali-activated binders, different precursors are used, such as ground-granulated blast-furnace slag (GGBFS), fly ash, metakaolin, etc. Each precursor has some advantages and disadvantages. For instance, GGBFS shortens setting time and reaches a high strength at an early age, but it also increases the possibility of forming cracks due to a large drying shrinkage [7]. Therefore, some approaches have been proposed to minimize its drawbacks, including using a combination of blended cements [8–12] and using fibers [13,14]. These efforts have been made mainly with two-part alkali-activated binders, however, leaving

---

a gap in the literature for assessing the efficiency of one-part alkali-activated binders.

As aforementioned, the main aim of alkali-activated binders is to maximize the use of recyclable materials in production of construction materials. To this end, some studies have indicated the potential of using recycled aggregate as a replacement for natural aggregates in alkali-activated binders [15–19]. One of these successful efforts used ceramic aggregates instead of natural aggregates in one-part alkali-activated binders [8], which had a low impact on the strength loss. In 2015, Ariffin et al. reported that using ceramic waste aggregate in a geopolymer concrete (with conventional, two-part alkali-activated binders) improved the compressive strength, flexural strength, and splitting tensile strength [20]. These results evince that ceramic waste aggregate is a useful component that should be considered in the design of high-strength geopolymer concrete. Waste ceramic could be a suitable aggregate in alkali-activated binders because it provides reactive silica, which is an essential component in the alkali-activation reaction to facilitate gel formation. In addition, using ceramic waste as the silica source has some ecological advantages, like conserving energy and natural resources, as well as reducing both the cost and the carbon footprint of the product [21].

Moreover, various studies have been conducted on using the benefits of fiber reinforcement of different alkali activated materials. The main focus in these studies was on alkali activated materials, which used lonely one precursor such as GGBFS or fly ash or metakaolin, and limited numbers of studies worked on the reinforcement of the blended alkaline binders. In the meantime, alkali activated fly ash/slag materials (as two-part) reinforced with different fibers such as steel [49,50,53–57], polypropylene (PP) [49,50], basalt [50,57], carbon [51,57], glass [57], and Polyvinyl alcohol (PVA) [52]. There is only one work regarding the tensile characterizations of fiber reinforced one-part alkali activated fly ash/GGBFS materials with hybrid combinations of steel and polyethylene fibers [58]. They reported that the precursor type, fiber type, and fiber content significantly affect the relative slump, density, fracture properties, and mechanical strengths. Additionally, it was found that the addition of fine natural aggregates (<0.2 mm) improve the fracture properties, while degraded the tensile strain capacity and multiple-cracking status [58].

So far, there is no study on the use of blended fly ash and GGBFS as precursors to balance the advantages and disadvantages of one-part alkali-activated binders with recycled ceramic aggregates. Moreover, the developed one-part alkali-activated slag/fly ash binders with ceramic aggregates (OAASFs) in this study were reinforced with PVA, PP, and basalt in single and hybrid combinations to enhance their mechanical and durability properties and reduce their drying shrinkage. Only one work has studied the influences of using ceramic aggregates; however, it was in one-part alkali-activated ceramic/slag binders [8].

The main aim was to develop fiber reinforced OAASFs with acceptable mechanical properties, low drying shrinkage, and acceptable freeze and thaw resistance. In order to achieve this point, it was initially required to develop the plain OAASFs with acceptable fresh and hardened state properties and comparable to those ones made with natural (or normal aggregates). Therefore, this paper was divided into two different stages, including the first stage of this paper was assigned to develop one-part alkali activated slag/fly ash binders containing ceramic aggregates with acceptable fresh and hardened state properties; then, the plain OAASF with the best performances in terms of fresh and hardened state properties was used to be reinforced with different fiber types (PVA, PP, basalt) and combinations (single and hybrid). Finally, the mechanical strength, drying shrinkage, and freeze and thaw resistance of OAASFs reinforced with different fibers were assessed.

## 2. Materials and mix designs

### 2.1. Raw materials

The raw materials in this study were GGBFS, a calcium-rich aluminosilicate precursor, and fly ash (FA), a binder rich in both silicon dioxide and aluminum oxide.

The GGBFS was provided by Finnsemetti (Finland), the $d_{50}$ value of which was 10.8 μm with a density of 2.93 g/cm$^3$. The dissolution of GGBFS is based on particle sizes; when larger than 20 mm, the particles react slowly, while smaller ones can react completely after 24 h in blended cements and alkali-activated binders [22,23]. Coal fly ash was obtained from Luja (Finnish Company). The $d_{50}$ value for the used fly ash was 21 μm.

The ceramic used in this work was porcelain ceramic waste (PCW), which totally replaced with natural sand. IDO (Finnish sanitary company) supplied the ceramic as a part of their waste. The detected crystalline phases were quartz 47.7%, mullite 48.9%, rutile 2.59%, and hematite 0.77%. The ceramic was crushed by using a jaw-mill, and the crushed material was sieved to reach a particle size between 0.5 and 4 mm. As mentioned earlier, natural aggregates (normal sand) were also used to compare the influence of ceramic waste as a recycled aggregate in alkali-activated binders. Standard sand was used as a natural aggregate in the first phase of the experimental plan using a sand-grain diameter distribution based on the ASTM D6913 recommendation [24] of between 0.08 and 2 mm. The sand-to-binder ratio was maintained at 2 based on the finding presented by Ghafoori et al. that the high strength in green concrete was achieved with this ratio [25].

Anhydrous sodium metasilicate ($Na_2O_3Si$, which provided from Alfa Aesar Company) with a silica modulus ($SiO_2/Na_2O$) of 0.9 and tap water with low hardness were used. It is worth mentioning that the particle size of solid sodium metasilicate was around 1 mm. In order to increase the chemical reactivity, the particles of solid sodium metasilicates were more grounded by using a miller for 10 min. Additionally, sodium metasilicates with other silica moduli of 0.9, 2.1, and 3.4 were used and let to obtaining the compressive strength of 103, 80, and 2 MPa, respectively [44]. Therefore, solid sodium metasilicate with silica modulus of 0.9 was chosen and used in this study.

The chemical compositions of GGBFS, FA, and PCW were determined by X-ray fluorescence (XRF) and are listed in Table 1. The XRF analysis was performed by a 4-Kv wavelength-dispersive XRF spectrometer (PANalytical AxiosmAX). The analyses were performed on the fused samples: 1.5 g of samples melted at 1150 °C with 7.5 g of X-ray Flux Type 66:34 (66% $Li_2B_4O_7$ and 34% $LiBO_2$) to obtain melt-fused tablets.

**Table 1**
The chemical compositions of GGBFS, FA, and PCW measured with XRF [%].

| Element/oxide, %, w/w | SiO$_2$ | AL$_2$O$_3$ | CaO | MgO | Fe$_2$O$_3$ | Na$_2$O | K$_2$O | TiO$_2$ | P$_2$O$_5$ | LOI |
|---|---|---|---|---|---|---|---|---|---|---|
| GGBFS | 32.33 | 9.58 | 38.51 | 10.24 | 1.23 | 0.00 | 0.53 | 0.00 | 0.01 | 1.20 |
| FA | 56.80 | 23.80 | 4.80 | 1.50 | 7.20 | 0.80 | 1.60 | 1.20 | 0.51 | 1.20 |
| PCW | 67.06 | 21.01 | 1.45 | 0.13 | 0.52 | 2.20 | 2.32 | 0.35 | 0.07 | n.a. |

## 2.2. Mix design

Different GGBFS/FA ratios were used, namely, 80:10, 60:30, 40:50, and 10:80 wt% in alkali-activated binders with natural or recycled aggregates. In total, ten different mix compositions were prepared and tested, including the reference samples. The mixtures designed are listed in Table 2. The individual system was used as a reference with GGBFS at 90 wt%. The reference mix composition (REFSN) was selected based on the developed mixture in [26].

## 2.3. Specimens synthesis and aging

The sample preparation and test procedure are as follows:

In the batching process, slag, fly ash, anhydrous sodium silicate and sand (standard sand or crushed ceramic waste) were initially combined and mixed for 3 min in a Kenwood industrial mixer at minimum speed. The tap water was added and stirred again for a further 3 min to ensure homogeneity. The molds were filled in two steps. First, they were half-filled and the shaker was used 60 times at a frequency of 1 impact per second. Then the molds were filled to the top and the shaker process was repeated. The fresh mortar was then poured and cast in prismatic beams (40 × 40 × 40 mm) to assess hardened-state properties.

The samples were labelled and put into an environment with controlled humidity and temperature for 24 h (the relative humidity [RH] at 60% and the temperature at 23 °C). The molds were stored in this controlled environment until the test date. In total, 30 prismatic beams were casted to assess the flexural strength. The portions of prisms broken during the flexural tests were used to assess the compressive strength, based on the ASTM C116-90 recommendation [27]. The specimens were tested after 7 and 28 days for flexural and compressive strength. The initial and final setting times were two of the main parameters to select a composition for use in real applications; these parameters were assessed and the results used to design the second phase of the experimental plan.

In the second phase of the experimental plan, the best receipt in terms of mechanical properties and setting time were selected.

The mix composition F3CW was used as the reference composition in the second phase of the experimental plan. In the second phase, the effects of different fiber types and combinations on the hardened-state properties were evaluated. As listed in Table 3, in total, 12 reinforced mix compositions were designed with three types of fibers (PP, PVA, and basalt) and two combinations (single and hybrid). The total amounts of fibers were kept constant (1.5% in volume) in all fiber-reinforced mixtures.

The main aim of this work was to develop construction materials, which stand against harsh conditions such as high temperature variations. Abdollahnejad et al. investigated the impacts of using different fibers (steel, PVA, cellulose, basalt) on the durability of one-part alkali activated slag based binders [45]. They reported that the reinforced one-part alkali activated slag based binders with steel fibers had the maximum strength loss (both flexural and compressive strength) and synthetic fibers had the minimum strength loss under cyclic freeze and thaw loadings. Moreover, PP fibers had great impacts on the reduction of the drying shrinkage of alkali activated materials. Therefore, these three fibers (PVA, PP, and basalt) were used to reinforce one-part alkali activated slag/fly ash binders.

The fiber-reinforced samples were prepared by the same casting procedure as the first phase of casting. The fibers were weighed and added gradually to prevent the formation of clumps after the water had been poured and mixed for one more minute. The fibers used in this thesis are listed in Table 4 along their relevant technical specifications. The values were provided by the manufacturers of the fibers.

## 2.4. Test procedure

### 2.4.1. Setting time

In accordance with the ASTM C807 – 18 recommendation, the initial and final setting time of the designed one-part alkali-activated mortars were measure using a Vicat apparatus [28]. The setting-time measurements were conducted at 20 °C and 60% RH. All mortars were cast in the standard cone using the mix design presented in Table 2 and used the same casting procedure. Based on the mentioned standard, the initial setting time is related to the time elapsed between the "zero time" and when the distance between the needle and the baseplate is 6 ± 3 mm. The final setting time is defined as the elapsed time, between the "zero time" and when the needle first penetrates 0.5 mm into the mortar. Fig. 1a shows the device used for measuring the initial and final setting times.

### 2.4.2. Drying shrinkage

According to the ASTM C157 recommendation, the drying shrinkage was determined by measuring the length change of the prismatic beams (40 × 40 × 160 mm) using a digital gauge with an accuracy within 0.001 mm [29]. Fig. 1b depicts the apparatus used for measuring the dry shrinkage. The specimens were exposed to the controlled environmental conditions (23 °C and 60% RH) one day after demolding. The drying shrinkage of each mixture was obtained by averaging the length changes of three replicate prismatic beams. Since the rate of length change immediately after demolding was relatively high,

**Table 2**
The designed mixtures for the plain OAASF.

| Mixture ID | Slag/binder* (%) | Fly ash/binder (%) | Sodium silicate/binder (%) | Water/binder (%) | Recycled ceramic waste/binder (%) | Normal aggregates/binder (%) |
|---|---|---|---|---|---|---|
| REFSN | 90 | 0 | 10 | 35 | 0 | 200 |
| REFCW | 90 | 0 | | | 200 | 0 |
| F1SN | 80 | 10 | | | 0 | 200 |
| F2SN | 60 | 30 | | | 0 | 200 |
| F3SN | 40 | 50 | | | 0 | 200 |
| F4SN | 10 | 80 | | | 0 | 200 |
| F1CW | 80 | 10 | | | 200 | 0 |
| F2CW | 60 | 30 | | | 200 | 0 |
| F3CW | 40 | 50 | | | 200 | 0 |
| F4CW | 10 | 80 | | | 200 | 0 |

Binder*: slag + fly ash + sodium silicate.

**Table 3**
The developed fiber reinforced mixtures.

| Mixture ID | Fiber type | Dosage of fiber (in Vol.) |
|---|---|---|
| 1.5PVA | PVA | 1.5% |
| 1.5PP | PP | |
| 1.5Ba | Basalt | |
| 0.5PVA1PP | PP + PVA | |
| 0.75PVA0.75PP | PP + PVA | |
| 1PVA0.5PP | PP + PVA | |
| 0.5PVA1Ba | Basalt + PVA | |
| 0.75PVA0.75Ba | Basalt + PVA | |
| 1PVA0.5Ba | Basalt + PVA | |
| 0.5PP1Ba | Basalt + PP | |
| 0.75PP0.75Ba | Basalt + PP | |
| 1PP0.5Ba | Basalt + PP | |

**Table 4**
The mechanical and physical properties of the used fibers.

| Fibre | Diameter (μm) | Cut length (mm) | Tensile strength (MPa) | Density (kg/m$^3$) |
|---|---|---|---|---|
| PVA | 40–200 | 8–18 | 1000–1600 | 1.30 |
| PP | 22.3 | 12 | 220–340 | 0.91 |
| Basalt | 18 | 25 | 4100–4840 | 2.80 |

the length variation was measured every two days and afterward, recording was measured every 3 to 7 days.

### 2.4.3. Mechanical properties

To investigate the effects of different ratios of GGBFS to FA and two types of sand on the development of the mechanical properties of the designed mortars, flexural and compressive strength were tested.

The prismatic beams (40 × 40 × 160 mm) were tested under three-point bending (TPB) in accordance with the ASTM C293 recommendation [30]. As shown in Fig. 1c, the flexural load was applied to the beams with a displacement rate of 0.6 mm/min.

The results were obtained from the average of three tested replicates.

Based on the ASTM C116-90 recommendation, the compressive strength was evaluated using the portions of prismatic beams broken in the flexural test [27]. All the broken prismatic beams were assessed under a compressive load with a constant displacement rate of 1.80 mm/min. The compressive load was measured with a Zwick Z100 Roell testing machine with a maximum load capacity of 200 kN. The results were obtained from the average of six tested replicates. It should be noted that multiple cracks did not form in the reinforced specimens under the flexural loading, therefore, the broken fiber reinforced specimens could be used for measuring the compressive strength.

### 2.4.4. Freeze-thaw assessment

Based on the ASTM C666 recommendation [31], three prismatic beams (40 × 40 × 160 mm) for each mix composition were prepared and tested. The test was performed with samples 28 days old. The specimens (samples) were immersed in water, ensuring that just half (20 mm) of each was in the water and the other half in the air, and then they were subjected to 120 freeze–thaw (F–T) cycles in a humidity chamber with temperatures ranging from −20 to + 15 °C. Cycles involved lowering the temperature of the samples from + 15 °C to −20 °C in 2 h and maintaining the temperature for another 2 h before increasing it back from −20 °C to + 15 °C for another 2 h and allowed to thaw for a final 2 h at 15 °C. After 120 cycles, the strength loss and weight of each sample was measured.

### 2.5. Microstructural analysis

#### 2.5.1. Scanning electron microscopy and X-ray spectroscopy

The chemical compounds and energy dispersion were identified using scanning electron microscopy (SEM) and X-ray spectroscopy (EDS), respectively.

For taking SEM images, small hardened parts of the selected mixtures were submerged in acetone to stop hydration before being carbon-coated. In this study, the SEM images (SEM-EDS, Zeiss Ultra Plus) were made with an acceleration voltage of 15 kV; the distance varied from 6 to 8 mm.

#### 2.5.2. X-ray diffraction

The mineralogical analysis was done using X-ray diffraction (XRD). The results were obtained from a Philips PW 1830 powder X-ray diffractometer, with Cu Kα (1.789 Å) radiation, a tube setting of 40 Kv and 40 Ma, a step size of 0.030°, a rate of 2.0 s per step and a 2Θ range of 10–70°. The phase identification was performed by Jade 7 software, version 5.1.2600, from Materials Data Inc.

#### 2.5.3. Thermogravimetric analysis and differential thermogravimetry

To study the conversion processes and reaction products at elevated temperatures, differential thermogravimetry (DTG) and a thermogravimetric analysis (TGA) were carried out on the 28-day samples using the Precisa Gravimetrics AG "prepASH automatic drying and washing system" The samples were crushed and heated to 1000 °C at 10 °C/min in a nitrogen atmosphere.

## 3. Development of the plain OAASF

### 3.1. Setting time

The initial ($T_i$) and final setting ($T_f$) times were assessed for each OAASF and the measurements were conducted according to the procedure proposed in the ASTM C807–18 recommendation. The results are presented in Fig. 2.

Based on the results, the replacement of slag by fly ash, regardless of sand type, increased the differences between the final and initial setting times. Retardation of the setting time can result from decreasing the total calcium content of the binder. The low rate of hydration caused by increasing the fly ash content, in contrast, prolongs the setting time. Moreover, increasing the fly-ash content of the total binder up to 60% continues to increase the difference between the final and initial setting times. Interestingly, replacement of fly ash more than 60% significantly increased both initial (more than 135 min.) and final (more than 180 min.) setting times, regardless of aggregate type.

Initial and final setting times of 20 and 28 min were recorded for the reference mixture with 90% slag, respectively, which is a short time for real applications based on the ASTM C807 – 18 recommendation. Thus, it was presumed that the replacement of up to 80% of the slag by fly ash could maximally prolong the setting time for fly ash and natural aggregates (F4SN).

Replacing fly ash up to 80% increased both initial and final setting times by a factor of 5 and 7, respectively, regardless of aggregate type. Moreover, when ceramic waste replaced with natural sand, it participated in the chemical reactions and thus shortened the setting time by up to 10%. Since ceramic wastes as recycled aggregates have higher porosity and absorb more water, this absorption increases the pH value of the alkali activator, which affects the setting time.

### 3.2. Flexural strength

Fig. 3a presents the flexural strengths of different OAASFs. For both natural and ceramic aggregates, decreasing the slag content consis-
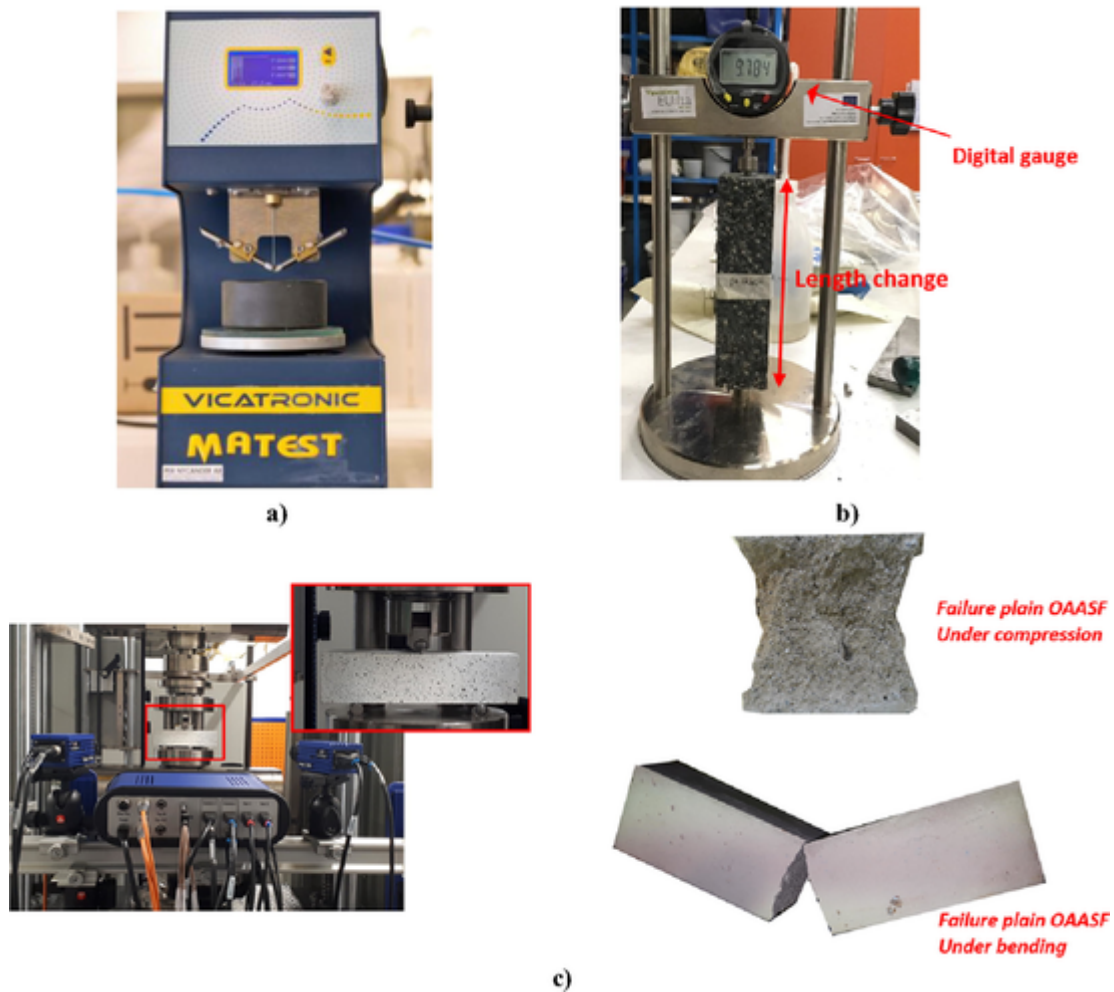
**Fig. 1.** The devices used for: a) measuring the initial and final setting times, b) measuring the length variation, and c) flexural test setup, and some failed prismatic and the halved beams under bending and compression tests.
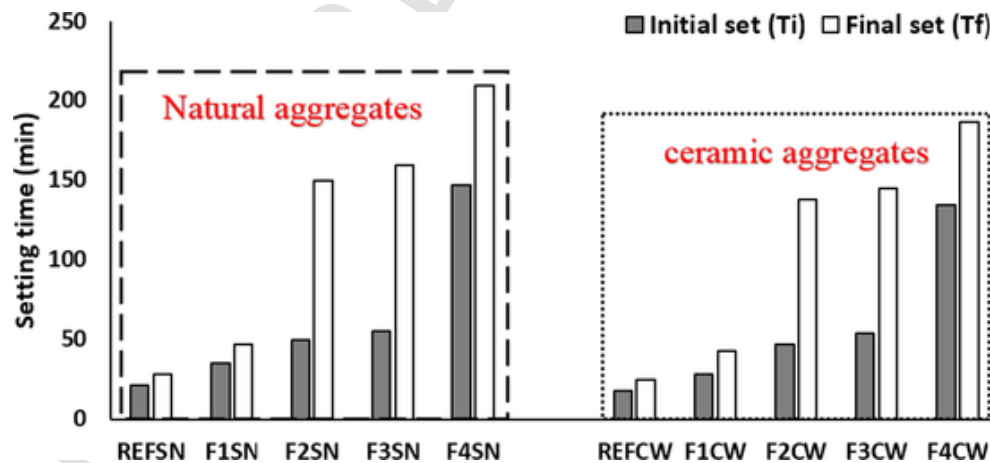


**Fig. 2.** The setting time of the designed mix compositions at room temperature.

tently reduces the flexural strength, although this trend is more pronounced in mixes with ceramic waste. Fig. 1c also shows the observed failure mode of prismatic beams made with the plain OAASF.

At both 7 and 28 days, regardless of aggregate type, the maximum reductions were around 50% for the mix in which 80% of slag was replaced with fly ash, as fly ash reduces the bonding properties of the matrix, both postponing the formation of chemical products and changing the chemical product types (the aluminium calcium silicate hydrate (C-A-S-H) gel to sodium- and aluminium-substituted calcium silicate hydrate (C/N-A-S-H) gel). The binding phases of alkali-activated materials depend on calcium content, including low, intermediate, and high [2]. The most important difference between the high calcium and low calcium alkali activated systems is that a substantial amount of $Ca^{2+}$ is dissolved from the solid source material [49,]. For the low content
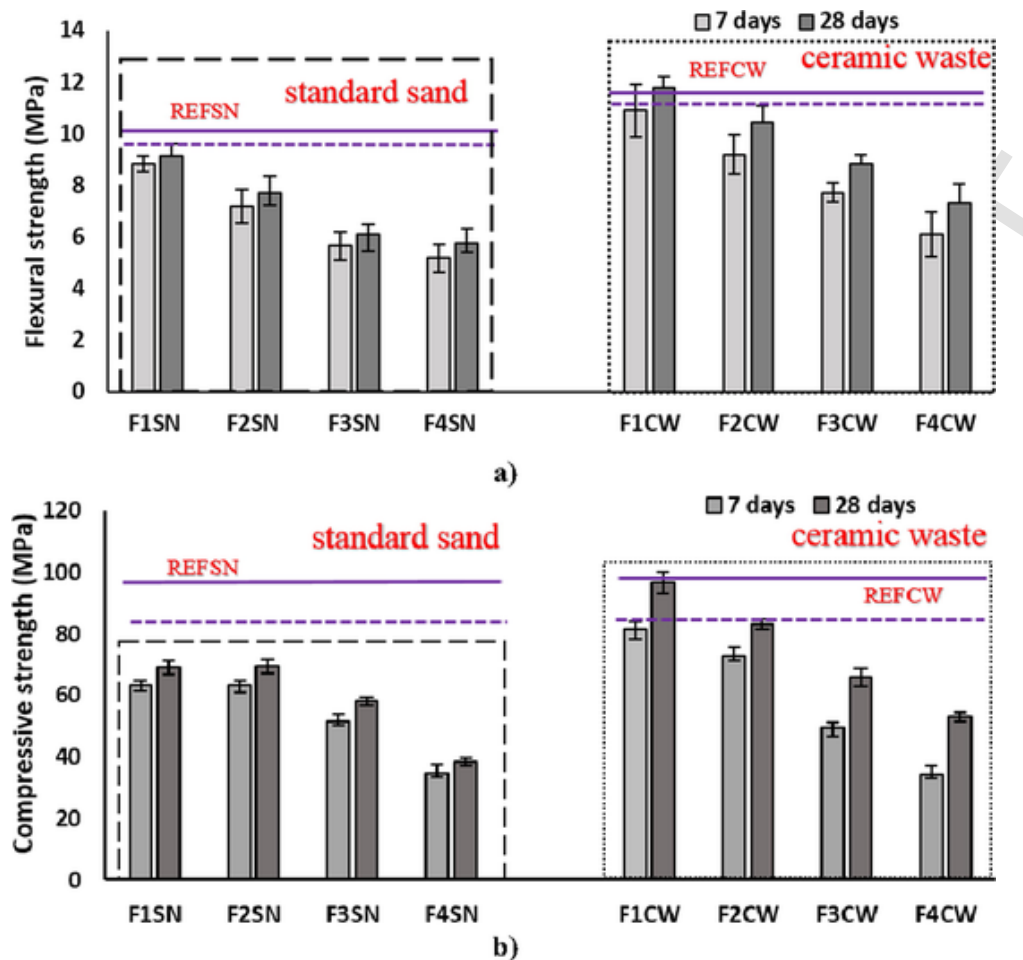
**Fig. 3.** The effects of using different contents of fly ash and sand types on the: a) flexural strength and b) compressive strength (violet, solid line: reference mixture at 28 days; violet, dashed line: reference mixture at 7 days). (For interpretation of the references to colour in this figure legend, the reader is referred to the web version of this article.)

of calcium, sodium aluminate silicate hydrate (N-A-S-H) gel is mainly formed. In high calcium alkali activated systems, both N-A-S-H and C-A-S-H gels are formed, which the hardening state properties depend on what gel-type becomes dominate [48]. The formation of C-A-S-H gel commonly shortens the setting time, improve mechanical strengths, and increase the drying shrinkage. Since the formation of N-A-S-H gel has an inverse trend.

The maximum and minimum increments due to the replacement of natural aggregate with ceramic waste were registered for F3CW (~45% at 28 days) and F4CW (~25% at 28 days), respectively. Ceramic aggregates are rich in aluminum and silica and participate in alkali activation, increasing the flexural strength in all mixes where it replaces natural aggregate.

Moreover, replacement of natural aggregates by ceramic aggregates has two more beneficial effects: 1) since ceramic has higher porosity than natural aggregates, it absorbs more free water, thus increasing the pH value and decreasing the liquid-to-binder ratio more than mixtures incorporating natural aggregates; 2) using recycled aggregates with a diameter less than 2 mm provides the best internal curing conditions and best water reservoir in alkali-activated slag binder because it reduces the water supply distance from the agent to the matrix [32,33].

The maximum flexural strength at both early (7 days) and final (28 days) ages were obtained around 11 MPa and 12 MPa, respectively, in a mix composition of 10% fly ash and ceramic waste (F1CW), while the minimum strengths were registered about 5 MPa and 6 MPa at the early and final ages, respectively, for the mix composition with 80% fly ash and natural aggregates (F4SN).

### 3.3. Compressive strength

Fig. 3b indicates the influences of replacing slag with fly ash and using ceramic wastes instead of natural aggregates on the compressive strength. Similar trends as those for flexural strength were noticed. Moreover, Fig. 1c indicates the failure mode of specimens under compression, which made with the plain OAASF.

The maximum strength loss was registered around 55% at both early and final ages in the mixes, in which 80% of slag was replaced by fly ash. Replacing slag with fly ash can reduce compressive strength by reducing the calcium content of the mix composition.

Compressive strength increased in all mixes, however, due to the replacement of natural aggregates by ceramic waste at both early and final ages, except the early age results for F3CW and F4CW.

As aforementioned, ceramic aggregates are rich in aluminum and silica, participate in alkali activation, increase the compressive strength, and absorb the available water in the mixture, which, in turn, increases the pH value, decreases the liquid-to-binder ratio, and beneficially influences internal curing due to their smaller grain size.

The benefits of replacing natural aggregates with ceramic wastes outweigh the strength loss from using fly ash instead of slag.

The highest compressive strength was achieved for the mix composition in which fly ash replaced 10% of slag and ceramic waste replaced standard sand, around 100 MPa at 28-day samples, while using 80% fly ash and natural aggregates only reached a compressive strength of around 40 MPa at 28 days.

Despite the strength loss from replacing slag with fly ash due to decreased calcium content, replacing natural aggregates with ceramic wastes compensates for this calcium reduction and increases the strength.

The obtained mechanical strengths from replacing natural aggregates with ceramic wastes are promising results in terms of mechanical, economical, and environmental benefits. Moreover, using fly ash instead of GGBFS efficiently prolonged the setting times and recognized mechanical strength in an appropriate range for being used as the construction applications.

### 3.4. Drying shrinkage

Limiting the negative effects of the drying shrinkage is an important aspect in cementitious systems; the most widely studied system is OPC. Generally, there are four types of shrinkage in concrete, mostly associated with OPC, but which are also relevant in alkali-activated systems. Drying shrinkage occurs as the volume changes due to the loss of moisture from the surface of the gel pores [34]. Because a high rate of shrinkage forms cracks and could consequently affect the durability properties and long-term performance of compositions, various studies have been conducted to avoid this phenomenon. Since alkali-activated binders are involved in many chemical processes, understanding the shrinkage behavior in these binders is more complicated than OPC compositions and is not yet understood properly [7]. Various investigations have been made to determine the effective parameters of the dry-

ing shrinkage in alkali-activated binders; however, information on the shrinkage behavior of these binder systems is scattered and fragmented.

Fig. 4 illustrates the impacts on the drying shrinkage of using either natural or ceramic aggregates and replacing GGBFS with fly ash. Using aggregates, regardless of type, reduced the drying shrinkage of the reference mixture matrix (90% GGBFS) without aggregate by more than a factor of four. It was also detected that the addition of aggregates (regardless of type) reached the drying shrinkage to stabilization at the earlier time than the reference matrix. As indicated in Fig. 4, some cracks formed on the surfaces of the prismatic beams made with the reference matrix, while no sign of cracks was observed in the OAASFs. In the mixtures with natural aggregates, replacing GGBFS with fly ash consistently increased the drying shrinkage by up to 50%, while the minimum drying shrinkage was recorded in the reference mixture (0.04 µε) with the maximum amount of GGBFS. These results are in the line of strength development. Using ceramic aggregates instead of natural aggregates, however, reverses this trend. Replacing GGBFS with fly ash by up to 30% increased the drying shrinkage, but increasing the percentage beyond this point actually reduced the drying shrinkage. The minimum drying shrinkage in the mixture containing fly ash and ceramic aggregates was recorded 0.017 µε in F3CW.

In general, it could be concluded that ceramic aggregates reduce the drying shrinkage more than natural aggregates. This finding could be due to: 1) the participation of the chemical components of ceramic aggregates in the chemical reactions; 2) the higher porosity and water demand of ceramic than natural aggregates, the available free water be-
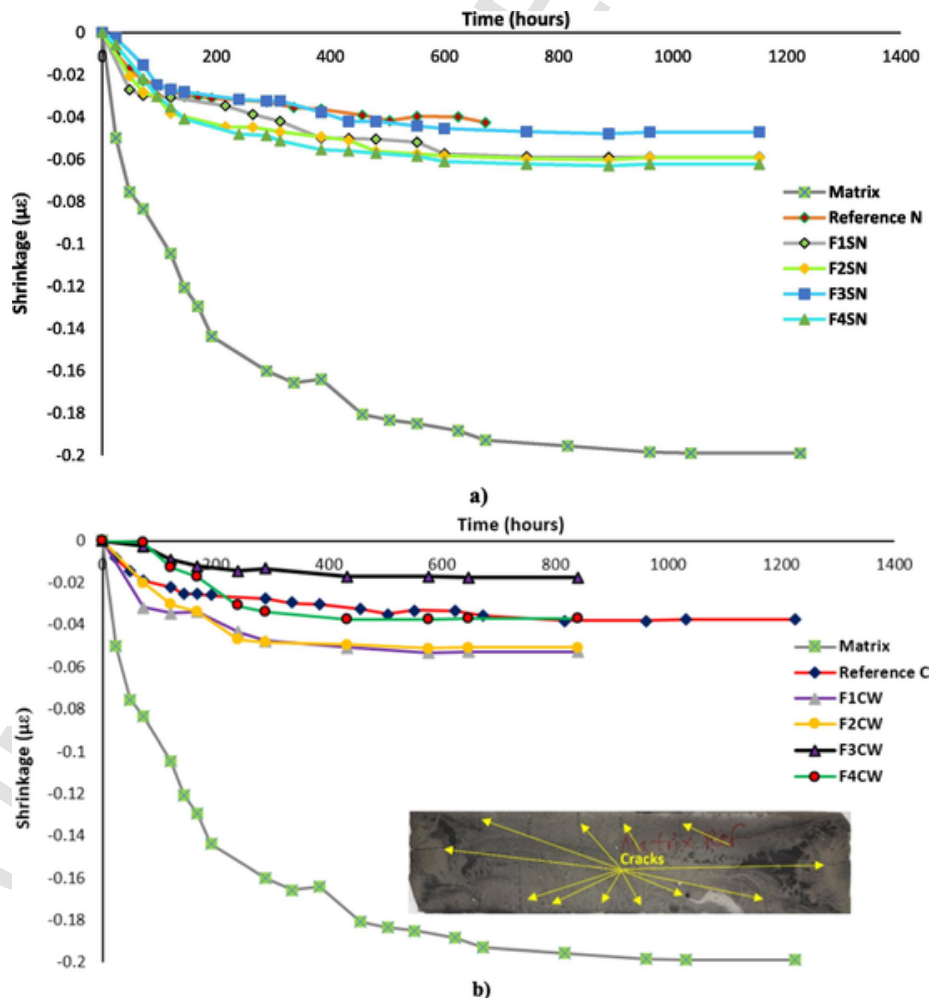


**Fig. 4.** The drying shrinkage of OAASFs with a) natural aggregates, and b) ceramic aggregates.

ing absorbed by ceramic aggregates, thus increasing the pH of alkali activators, reducing the liquid-to-binder ratio, and increasing the strength; and 3) the effect of their smaller grain size on the internal curing mechanisms.

### 3.5. SEM/EDS analysis

Since one of the main aims of this investigation was maximizing the use of recycled materials in alkali-activated materials, the microscopic analysis investigated the influences of ceramic waste as aggregates in OAASF. The morphologies of the designed mix compositions with different ratios of GGBFS/fly ash and ceramics aggregates are presented in Fig. 5. Moreover, molar ratios for these mixtures have been presented in Fig. 6 based on EDS analysis. EDS analysis was carried out based on the data obtained from the matrix.

According to the EDS analysis in Fig. 6, using fly ash as replacement for slag decreased the calcium and silicon oxides, which directly affected the strength of the designed mix compositions. A higher level of $Cao/SiO_2$ justifies the higher compressive strength of the mix compositions with a higher content of slag in the binder system. The forma-

tion of some micro-cracks in the interfacial transition zone (ITZ) between the ceramic aggregate and the matrix, detected in Fig. 5a, could be due to the high level of shrinkage in the formed gels. The morphology of the mixtures changed by replacing slag with fly ash so that the porosity of the matrix and the number of unreacted fly-ash particles both increased (see Fig. 5e). This can be justified by the lower mechanical strength of the mixes with higher contents of fly ash.

### 3.6. XRD analysis

The mineral patterns of the mixtures containing natural aggregate and ceramic waste are shown in Fig. 7. A comparative XRD analysis was performed in this phase to evaluate the effects of ceramic waste and fly ash on the formation of different crystals in developed OAASFs.

The results showed that similar XRD patterns formed in the mixtures, although different precursor contents can affect the intensity characteristics of the formed diffraction peaks. Changing the aggregate type from natural aggregates to ceramic waste significantly increased the crystallization and some new crystals formed (quartz and dolomite to quartz, calcite, and mullite), which could affect the mechanical strength of the mix compositions with ceramic waste.
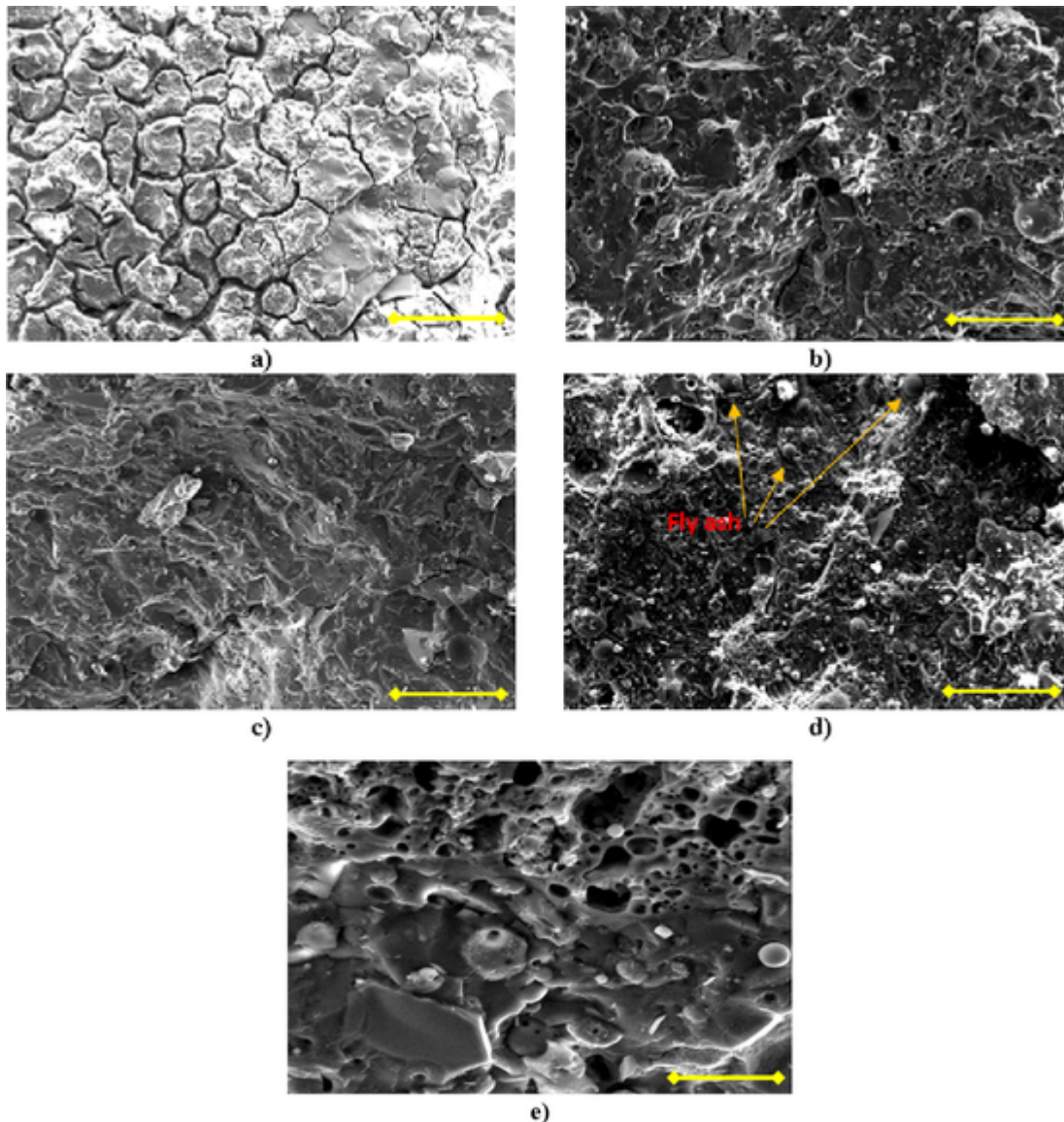


**Fig. 5.** The SEM images taken from five different mix compositions with *300X* magnification: a) REFCW; b) F1CW; c) F2CW; d) F3CW; and e) F4CW.
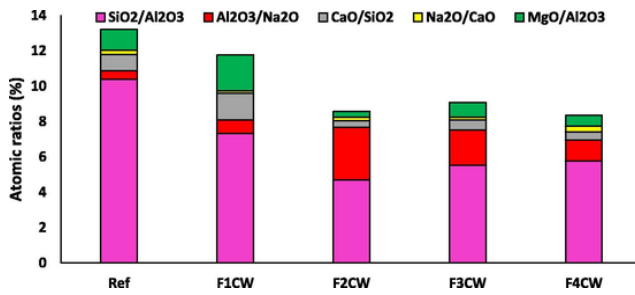
**Fig. 6.** The EDS atomic ratios of the mix compositions.

Huseien et al. showed that semi-crystalline aluminosilicates gel and quartz are observed in alkali activated mortars containing ceramic wastes, GGBFS, and FA [46]. Different contents of ceramic wastes, GGBFS, and FA effect on the formation of new crystals in alkali activated materials. Under high temperature (700 °C), the main identified peaks were concerned with quartz, mullite, and nepheline, which both mullite and quartz were recognized as stable crystalline phases [46].

As aforementioned, ceramic aggregates participate in the chemical reactions and increase the crystallinity. This observation is in line with findings in [8,47]. Ceramics affect the characteristic diffraction peaks and the formed crystallinity phases in alkali activated binders [8,47].

Increasing crystallinity can either increase or decrease certain mechanical properties, depending on the availability of space in the mixture to be filled with crystals. Moreover, the transition of amorphous gels to ordered structures can cause internal stress due to changing the microstructure [35]. The improvement in mechanical strength made by replacing natural aggregates with ceramic wastes could have caused the irregular shape of the crushed ceramic wastes, increasing the porosity and thus providing enough space for the crystal formation.

### 3.7. TGA/DTg

One of the main aim of this work is to replace natural aggregates with ceramic aggregates. To this end, the impacts of ceramic wastes on the morphology and mineralogy were studied, the results of which are presented in this section. Fig. 8 depicts the mass loss and the derivative mass of mix compositions with different fly-ash contents.

Both TGA and DTG were used to identify the reaction products at high temperatures (see Fig. 8). Mass losses in TGA were observed from 100 to 800 °C [36]. Mass loss below 100 °C is mostly attributed to the evaporation of capillary pore water and phases with bounded water [37]. Mass loss from 100 to 800 °C is attributed to the structural water [37].

The results in Fig. 8a show that mass loss was higher in the mix compositions with lower amounts of slag, which agrees with the strength reduction of slag being replaced by fly ash [9].

Based on the DTG results in Fig. 8b, one main endothermic peak was detected between 180 and 200 °C that could be attributed to the presence of the aluminium calcium silicate hydrate (C-A-S-H) gel. The mass loss rate slowed down after 250 °C owing to the chemically bonded water and OH groups [37]. The second destruction phase (at 600 °C) could be attributed to the decomposition of calcium hydroxide (Ca(OH)$_2$) [38,39]. The differences in the major endothermic peaks indicate that some additional gel formation may have occurred owing to different fly-ash contents.

## 4. Development of fiber-reinforced OAASF

In the second stage of this paper, the impacts of using different fiber types and combinations on the mechanical performances, drying shrinkage, and freeze/thaw resistance were investigated. These assessments were performed on the 28-day-old specimens.

According the results presented in the first phase of this paper, the mixture F3CW was selected to be reinforced with different fibers
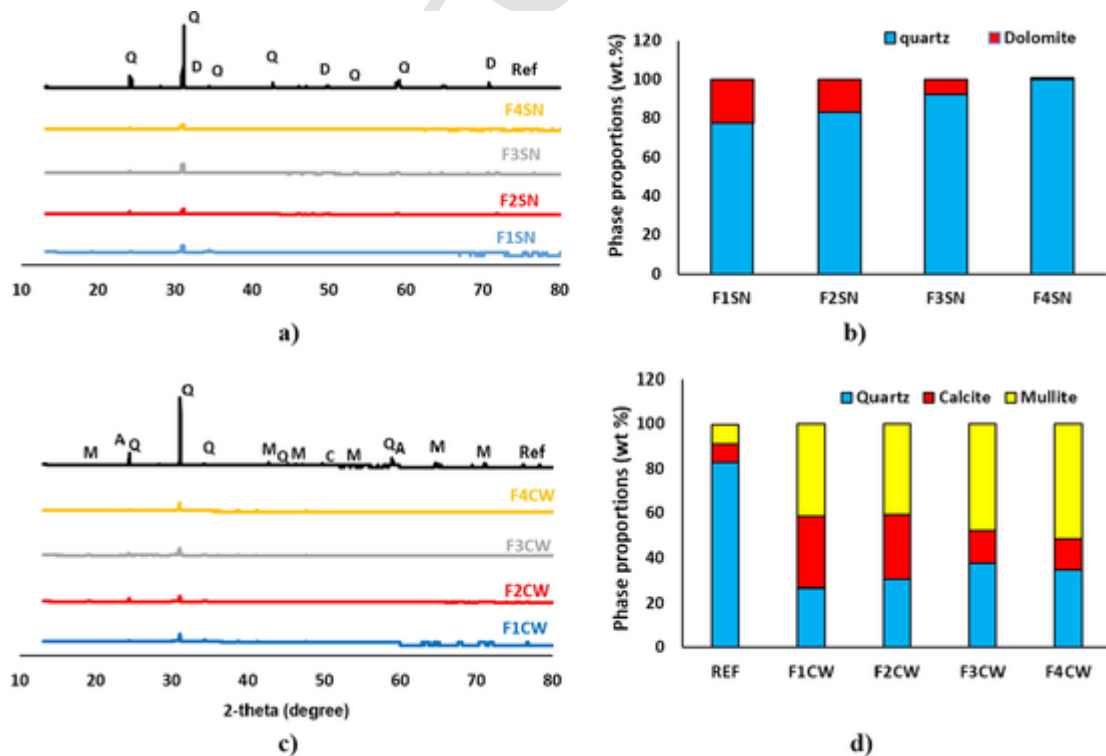


**Fig. 7.** The XRD patterns and phase proportions of mixtures with a) & b) natural aggregates (Quartz; D: Dolomite) and c) & d) ceramic waste (Quartz; C: Calcite; M: Mullite).
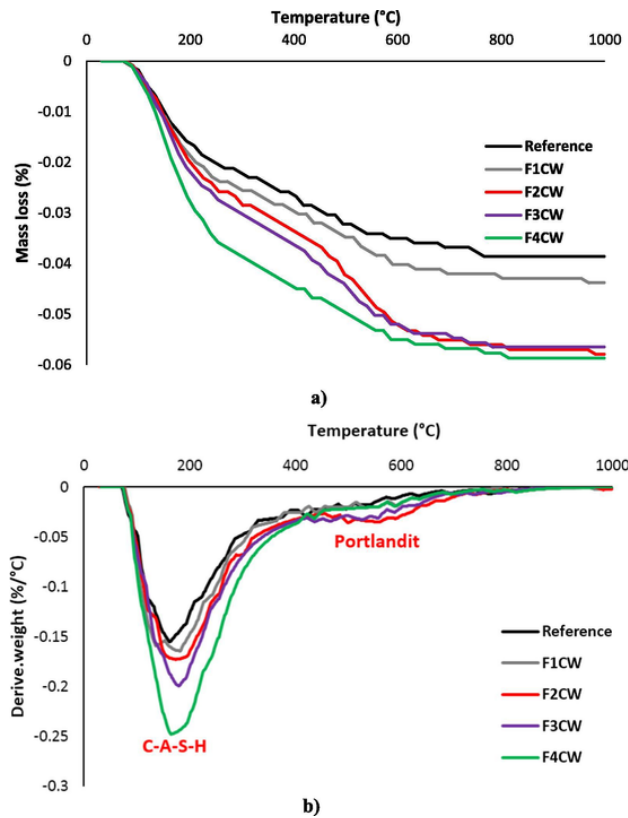
**Fig. 8.** a) The TGA of one-part slag/fly ash alkali-activated mortars containing ceramic waste and b) The DTG analysis of OAASF containing ceramic waste.

and fiber combinations. This mixture was selected based on high strength, low drying shrinkage, and long setting time.

Since the addition of fly ash to the mixture hinders the formation of chemical products, the strength development of the reinforced mixtures was evaluated after 28 and 90 days.

### 4.1. Flexural strength

Fig. 9b displays the impact of reinforcing the prismatic beams on the flexural strength. The flexural strength results showed that it can be influenced by different types and combination of fibers. As mentioned earlier, the addition of fibers can increase the number of cracks because of fiber-bridging action [40]. The flexural strength after 28 days increased in all mixtures by adding fibers, except in mixes that were reinforced (1.5PP and 0.5PVA1PP). In the reinforced OAASF with single-PP fibers, the reduction of flexural strength was mainly due to a weak bond at the fiber/matrix ITZ during deboning [41]. Moreover, the strength reduction in the reinforced OAASF with hybrid PP and PVA fibers could be due to the synergistic impacts of PP and PVA fibers. After 28 days, the gain of the flexural strength in the reinforced OAASF with single fibers was limited to ~30%, while this increase for the hybrid combination reinforcement is ~25%.

The maximum flexural strength (~35%) for the single fibers was observed in a mix reinforced with 1.5%BA after 90 days. The maximum flexural strength (~30%) for hybrid combinations was observed in the mix composition with 0.5%PVA and 1%BA.

After long-term curing (90 days), the flexural strength rose above the strength at 28 days, showing that the formation of chemical products filled the gaps at the fiber/matrix ITZ and improved the bond properties. The time of curing has significant impacts on strength development. Nevertheless, in general, it can be concluded that the flex-

ural strength mainly depends on the fiber combination and fiber content rather than the period of curing.

### 4.2. Compressive strength

The influences on the compressive strength of reinforcing OAASF with different fiber types and combinations is depicted in Fig. 9a. The effect of adding fibers on the compressive strength can be either positive or negative. The compressive strength rises when fibers arrest crack propagation, but it falls when fibers create more air voids [6].

Based on the results, a greater decline was registered for all the reinforced mix compositions after 28 days than for the reference mix composition. This strength loss could be due to the increased porosity caused by more fibers [42]. The maximum decrease (~70%) was observed in the mixed compositions (1PVA0.5PP, 1PVA0.5BA, 0.75PP0.75BA). Comparing the 28-day and 90-day results showed that adding fibers resulted in long-term gains in compressive strength, possibly due to gradually filling air voids with chemical products. The reduction of porosity leads to increase interaction for fibers during debonding. Based on this phenomenon, the maximum increase of the compressive strength in the reinforced mixtures with single fibers was observed in 1.5PP (~10%).

Moreover, based on the results, the maximum increase of the compressive strength after 90 days was around 60% in the hybrid fiber-reinforced mix compositions (0.75PP0.75PVA, 0.75PVA0.75BA, and 0.75PP0.75BA) compared to 28-day curing. In general, using hybrid fibers have higher impacts on increasing the compressive strength than single fibers after 90 days curing.

Increasing the curing time from 28 to 90 days for the reference mix composition without fiber led to obtaining the minimum increase in the compressive strength (~1%). This small increase is related to the reaction of the unreacted particles (mainly related to fly ash).

### 4.3. Drying shrinkage

One of the easiest and most effective ways to mitigate the negative impacts of a large drying shrinkage is to reinforce the mixtures with fibers, although the efficiency of this technique is significantly governed by fiber type, content, and their physical and mechanical properties [7]. Fig. 10 displays the influences of different fiber types and combinations on the drying shrinkage. Interestingly, the addition of most fibers increased the drying shrinkage more than the plain mixture. The only effective fiber in reducing the drying shrinkage was 1.5BA, which mitigated approximately 15% of the ultimate drying shrinkage. Although the addition of all hybrid combination fibers increased drying shrinkage, the minimum increase was recorded (~10%) in 0.5BA1PP. Despite the increase of the drying shrinkage in most reinforced mixtures compared to the plain reference mixture, the recorded ultimate drying shrinkage (0.05 με) is even lower than some of the plain mixtures developed in the first phase of this paper. Moreover, the recorded drying shrinkages in the plain and reinforced OAASFs are much lower than the value, which cracks were observed in the matrix (0.2 με).

## 5. Freeze-thaw resistance

Freeze-thaw resistance depends on the tortuosity, pore distribution, and pore-size volume of OAASFs. A higher level of water suction generates greater ice-volume formation inside the pores; this expansion submits to the compressive load on the matrix walls, while melting unloads this imposed internal stress and decreases the pore volume. The final volume change of the pores depends on the elastic/plastic strains (i.e., the permanent/recovered deformations) of the matrix, although pore sizes become larger and total porosity increases after performing this test. This type of loading/unloading due to expansion/contraction of the volume could be simulated as fatigue loading [40,43,45]. More-
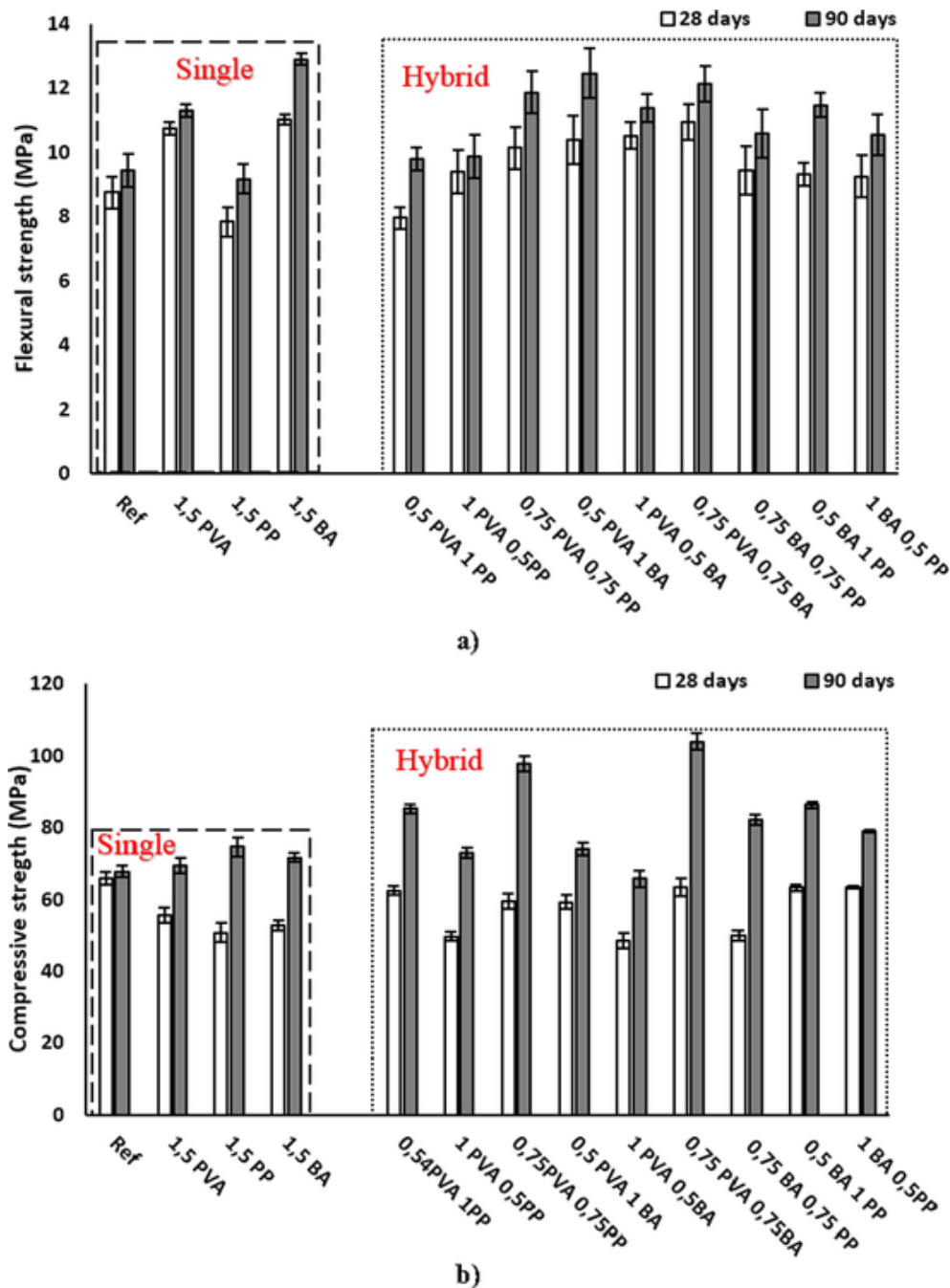
Fig. 9. The mechanical properties of the reinforced OAASF: a) flexural strength and b) compressive strength.

over, the addition of fibers can engender two scenarios regarding freeze-thaw resistance: 1) increased porosity and 2) fiber-bridging action. Furthermore, it should be noted that the efficiency of fiber-bridging action is influenced by the pores at the fiber/matrix ITZ. Filling these pores with water and exposing them to freeze-thaw, loading/unloading cycles degrades the bonding properties of the fiber/matrix ITZ. Moreover, it should be noticed that pores' distribution and size inside of the matrix can be governed by fiber type, fiber distribution, and fiber content (these parameters affect the fiber dispersion). Therefore, the suction of water and impacts of loading/unloading due to expansion/contraction of the volume could be different in the reinforced OAASFs.

The resistance of the reinforced OAASFs in freeze/thaw conditions was observed by partially submerging specimens in water. This test was designed for 120 freeze–thaw cycles; the compressive and flexural strengths were measured after the cycles finished. The weight losses of the samples were measured and are presented in Fig. 11a.

Based on the results, all the tested samples showed high resistance to the freeze–thaw cycles, although they all experienced mass loss to some extent. The results show that around 5% mass loss was registered in a reference OAASF. The mass loss in the reinforced OAASFs was limited to 3.5%, so that the minimum mass loss was registered at around 0.4% for the reinforced mix composition with 1.5% Basalt fiber. The mass loss shows that using fibers can improve the integrity of the alkali activated materials under freeze/thaw conditions.

Fig. 11b & c depict the compressive and flexural strengths of the reinforced mix compositions before and after being exposed to 120 freeze–thaw cycles, respectively. As it was expected, the compres-
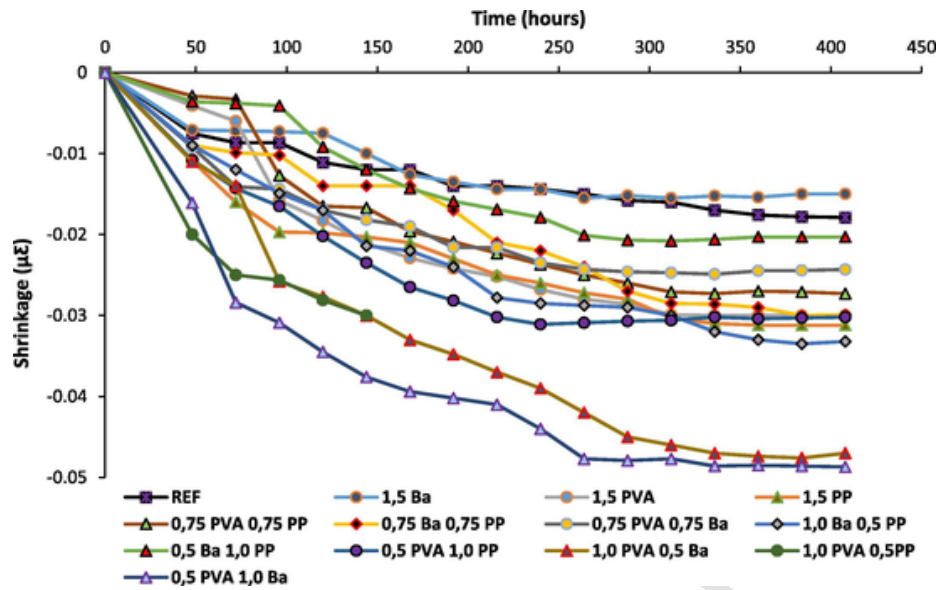
**Fig. 10.** The effects of using different fiber types and combinations on the drying shrinkage.

sive and flexural strengths dropped in all the mix compositions. Based on the results, around 10% and 25% reductions in compressive and flexural strength were registered for the plain mix compositions, respectively.

According to the results presented in Fig. 11b, the minimum and maximum compressive strength loss with single-fiber reinforcement were registered at around 10% for 1.5PVA and around 15% for 1.5PP. Moreover, for hybrid fiber reinforcement, the maximum and minimum compressive strength reductions were registered at around 50% and 15% in reinforced mix compositions for 0.75 PVA 0.75PP and 0.5 PVA 1BA at 90 days, respectively. Referring to the results presented in Fig. 11c, the minimum and maximum flexural strength reductions in the single-fiber reinforced mix compositions were around 10% for 1.5PVA and around 30% for 1.5PP. In addition, for hybrid fiber reinforcement, the maximum and minimum flexural strength reductions were registered at around 50% and 10% in the two reinforced mix compositions (0.75PVA 0.75BA & 0.75PP 0.75BA; 0.5PP1BA & 0.5PVA1BA) at 90 days, respectively.

In general, it can be concluded that single-fiber reinforcement has better performance in limiting the strength loss than hybrid combination reinforcement under freeze/thaw conditions. This conclusion comes from differences in the pores' distribution and size inside of the matrix, which provided by different fiber combinations and types. These parameters generate some differences in water suction and impacts of loading/unloading due to expansion/contraction of the volume of fiber-reinforced OAASFs.

Fig. 12 illustrates the embedded fibers in the matrix and fiber failure modes. These images were taken from the fracture surface of specimens. According to these images, PVA and basalt fibers provided excellent bond at ITZ between fiber and matrix, and the matrix has been attached to the surfaces of the fibers. In this case, as expected, fibers were ruptured. Due to smooth surfaces of PP fibers, these fibers provided weak bond properties at fiber/matrix and consequently, PP fibers were debonded from their surrounded matrix and paths were created, as shown in Fig. 12b.

## 6. Conclusion

This experimental study investigated the influences of replacing natural aggregates with ceramic aggregates and replacing GGBFS with fly ash on both the fresh and hardened-state properties of OAASFs. Afterward, one mixture was chosen from a reference OAASF, and then dif-

ferent fiber types and combinations were used to reinforce its mechanical properties, reduce its drying shrinkage, and improve its freeze–thaw resistance. According to the results, the following remarks could be made:

1. Replacing natural aggregates with ceramic aggregates has no negative impact on the setting time. Moreover, using a composition of above 60% fly ash instead of GGBFS significantly increases the setting times (more than 135 min. for the initial and 180 min. for the final setting time).
2. Replacing GGBFS with fly ash consistently reduces mechanical strength (35–40% reduction in the flexural strength and 45% loss for the compressive strength), although using ceramic aggregates instead of natural aggregates can compensate for these strength losses (25–45% increase of the flexural strength and 15–40% increase for the compressive strength). However, OAASF with maximum fly ash content (80%) and fully replacement of natural aggregates with ceramic aggregates (F4CW) provided acceptable mechanical strength ($<7$ MPa flexural strength and $<50$ MPa compressive strength) and setting time ($<135$ min. for the initial and $<180$ min. for the final setting time) for being used in the construction applications.
3. Regardless of aggregate type (natural or ceramic), the use of aggregates reduces the drying shrinkage of the reference matrix without aggregates by more than a factor of four. Moreover, in general, larger drying shrinkage was observed in alkali-activated binders with natural aggregates than ones with ceramic aggregates.
4. The minimum drying shrinkage in the plain OAASF was recorded at 0.017 με in the F3CW. Except for 1.5BA, all the fiber types and combinations increased the drying shrinkage; the minimum drying shrinkage in the reinforced OAASF with 1.5BA was registered at around 0.015 με, which was approximately 15% lower than the ultimate drying shrinkage of the plain F3CW.
5. Four mechanisms contributed to the better performances of the hardened-state properties of OAASFs containing ceramic aggregates instead of natural aggregates: 1) the participation of the chemical components of the ceramic aggregates in the chemical reactions; 2) the higher porosity and water demand of ceramic than natural aggregates and the available water absorbed by the ceramic aggregates, which increases the pH of the alkali activator, reduces the liquid-to-binder ratio, and increases its strength; and 3) the effect
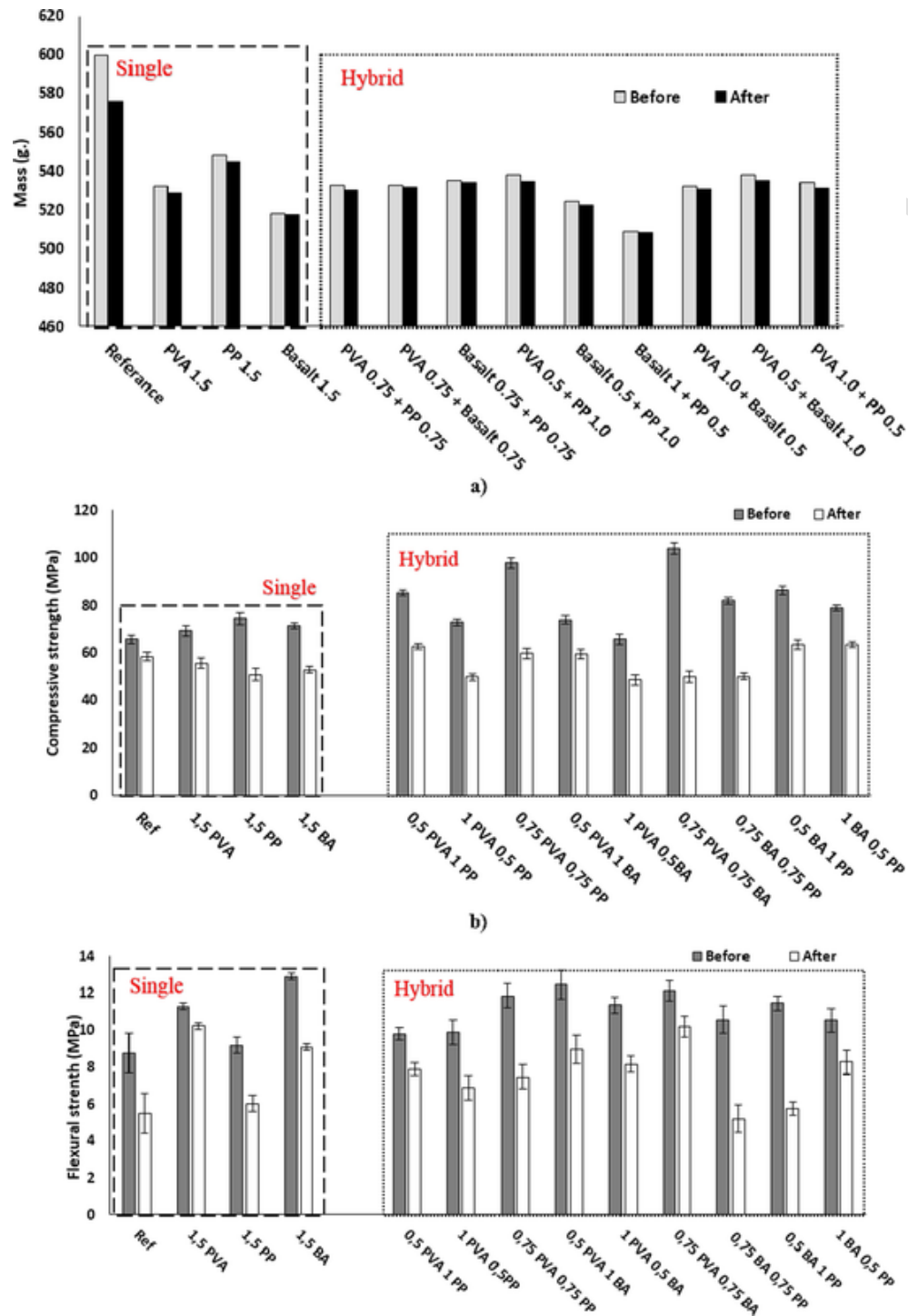
**Fig. 11.** The effects of freeze-thaw cycles on the a) mass loss, b) compressive strength, and c) flexural strength.

of the smaller particle size of the ceramic aggregates on the internal curing mechanisms.

6. In general, after 90 days of curing, hybrid fibers (<50% increase) increase the compressive strength more than single fibers (~10% increase). Since single-fiber reinforcement had higher flexural strength gain (~35%) than hybrid combination reinforcement (~30%).

7. A low mass loss (0.4–3.5%) indicates that using fibers improves the integrity of the mixtures after 120 freeze–thaw cycles. Single-fiber reinforcement has better performance in limiting the strength loss (10–15% for compressive strength loss and 10–30% reduction in the flexural strength) than hybrid combination reinforcement (15–50% compressive strength loss and 10–50% reduction for the flexural strength) under freeze/thaw conditions. The best performance in terms of the minimum observed mechanical strength loss was for 1.5PVA with a 10% mechanical strength loss (for both compressive and flexural strengths).
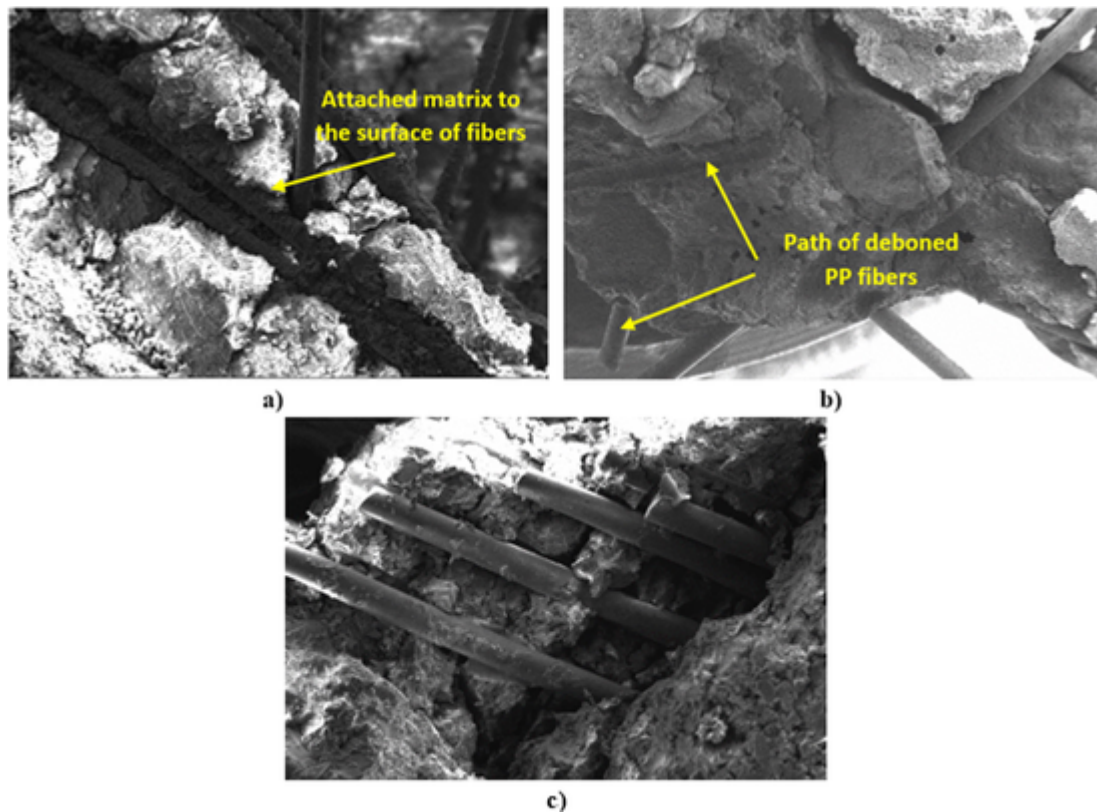
**Fig. 12.** SEM images from the mixture reinforced with: a) basalt fiber, b) PP fiber, and c) PVA fiber.

## CRediT authorship contribution statement

**Z. Abdollahnejad:** Conceptualization, Methodology, Writing - review & editing. **M. Mastali:** Conceptualization, Methodology, Writing - review & editing. **B. Woof:** Writing - review & editing. **M. Illikainen:** Writing - review & editing, Supervision.

## Declaration of Competing Interest

The authors declare that they have no known competing financial interests or personal relationships that could have appeared to influence the work reported in this paper.

## Acknowledgments

## References

[1] J. Davidovits, Global warming impact on the cement and aggregates industries, World Res. Rev. 6 (2) (1994) 263–278.

[2] T. Luukkonen, Z. Abdollahnejad, J. Yliniemi, P. Kinnunen, M. Illikainen, One-part alkali-activated materials: a review, Cem. Concr. Res. 103 (2018) 21–34.

[3] J. Provis, Alkali-activated materials, Cem. Concr. Res. 114 (2018) 40–48.

[4] F. Pacheco-Torgal, J. Castro-Gomes, S. Jalali, Alkali-activated binders: A review Part 1. Historical background, terminology, reaction mechanisms and hydration products, Constr. Build. Mater. 22 (2008) 1305–1314.

[5] F. Pacheco-Torgal, J. Castro-Gomes, S. Jalali, Alkali-activated binders: A review. Part 2. About materials and binders manufacture, Constr. Build. Mater. 22 (2008) 1315–1322.

[6] Z. Abdollahnejad, M. Mastali, T. Luukkonen, P. Kinnunen, M. Illikainen, Fiber-reinforced one-part alkali-activated slag/ceramic binders, Ceram. Int. 44 (2018) 8963–8976.

[7] M. Mastali, P. Kinnunen, A. Dalvand, F.R. Mohammadi, M. Illikainen, Drying shrinkage in alkali-activated binders – A critical review, Constr. Build. Mater. 190 (2018) 533–550.

[8] Z. Abdollahnejad, T. Luukkonen, M. Mastali, P. Kinnunen, M. Illikainen, Development of one-part alkali activated ceramic/slag binders containing recycled ceramic aggregates, J. Mater. Civ. Eng. (2018), doi:10.1061/(ASCE)MT.1943-5533.0002608.

[9] Z. Abdollahnejad, T. Luukkonen, M. Mastali, C. Giosue, O. Favoni, M.L. Ruello, P. Kinnunen, M. Illikainen, The microstructural analysis and strength development of one-part alkali slag/ceramic activated binders under different curing regimes, Waste Biomass Valorization (2019), doi:10.1007/s12649-019-00626-9.

[10] M. Nedeljković, Z. Li, G. Ye, Setting, strength, and autogenous shrinkage of alkali-activated fly ash and slag pastes: Effect of slag content, Materials 11 (2018), doi:10.3390/ma11112121.

[11] N.K. Lee, H.K. Lee, Reactivity and reaction products of alkali-activated, fly ash/slag paste, Constr. Build. Mater. 81 (2015) 303–312.

[12] J.E. Oh, M.P. Paulo, S.S. Jun, S. Choi, S.M. Clark, The evolution of strength and crystalline phases for alkali-activated ground blast furnace slag and fly ash-based geopolymers, Cem. Concr. Res. 40 (2010) 189–196.

[13] N. Ranjbar, S. Talebian, M. Mehrali, C. Kuenzel, H.S.C. Metselaar, M.Z. Jumaat, Mechanisms of interfacial bond in steel and polypropylene fiber reinforced geopolymer composites, Compos. Sci. Technol. 122 (2016) 73–81.

[14] N. Ranjbar, M. Mehrali, M. Mehrali, U.J. Alengaram, M.Z. Jumaat, High tensile strength fly ash based geopolymer composite using copper coated micro steel fiber, Constr. Build. Mater. 112 (2016) 629–638.

[15] M. Mastali, Z. Abdollahnejad, F. Pacheco-Torgal, Performance of waste based alkaline mortars submitted to accelerated carbon dioxide curing, Resour. Conserv. Recycl. 129 (2018) 12–19.

[16] M. Mastali, Z. Abdollahnejad, F. Pacheco-Torgal, Carbon dioxide sequestration of fly ash alkaline-based mortars containing recycled aggregates and reinforced by hemp fibres, Constr. Build. Mater. 160 (2018) 48–56.

[17] M. Mastali, Z. Abdollahnejad, F. Pacheco-Torgal, Carbon dioxide sequestration on fly ash/waste glass alkaline-based mortars with recycled aggregates: Compressive strength, hydration products, carbon footprint and cost analysis, Carbon Dioxide Sequestration Based Cementitious Construction Materials, Ed. Pacheco-Torgal, Shi & Palomo, 1–15. Abington Hall, Woodhead Publishing Ltd-Elsevier Science and Technology, Cambridge, 2018.

[18] P. Nuaklong, V. Sata, P. Chindaprasirt, Properties of metakaolin-high calcium fly ash geopolymer concrete containing recycled aggregate from crushed concrete specimens, Constr. Build. Mater. 161 (2018) 365–373.

[19] M. Bassani, L. Tefa, A. Russo, P. Palmero, Alkali-activation of recycled construction and demolition waste aggregate with no added binder, Constr. Build. Mater. 205 (2019) 398–413.

[20] M.A. Ariffin, M.W. Hussin, M. Samadi, N.H. Lim, J. Mirza, D. Awalludin, N. Othman, Effect of ceramic aggregate on high strength multi blended ash geopolymer mortar, Jrnal Teknologi 77 (16) (2015) 33–36.

[21] F. Pacheco-Torgal, S. Jalali, Compressive strength and durability properties of ceramic wastes based concrete, Mater. Struct. 44 (2010) 155–167.

[22] J.J. Chang, A study on the setting characteristics of sodium silicate-activated slag pastes, Cem. Concr. Res. 33 (2003) 1005–1011.

[23] H. Wan, Z. Shui, Z. Lin, Analysis of geometric characteristics of GGBS particles and their influences on cement properties, Cem. Concr. Res. 34 (2004) 133–137.

[24] ASTM D6913/D6913M-17, Standard Test Methods for Particle-Size Distribution (Gradation) of Soils Using Sieve Analysis, ASTM International, West Conshohocken, PA, 2017, www.astm.org.

[25] N. Ghafoori, M. Najimi, B. Radke, Natural Pozzolan-based geopolymers for sustainable construction, Environ. Earth Sci 75 (2016) 1110, doi:10.1007/s12665-016-5898-5.

[26] T. Luukkonen, Z. Abdollahnejad, J. Yliniemi, P. Kinnunen, M. Illikainen, Comparison of alkali and silica sources in one-part alkali-activated blast furnace slag mortar, J. Cleaner Prod. 187 (2018) 171–179.

[27] ASTM C116–90, Test Method for Compressive Strength of Concrete Using Portions of Beams Broken in Flexure, ASTM International, West 1990 Conshohocken, PA www.astm.org.

[28] ASTM C807-18, Standard Test Method for Time of Setting of Hydraulic Cement Mortar by Modified Vicat Needle, ASTM International, West Conshohocken, PA, 2018, www.astm.org

[29] ASTM C157/C157M–17, Standard Test Method for Length Change of Hardened Hydraulic-Cement Mortar and Concrete, ASTM International, West 2017 Conshohocken, PA www.astm.org.

[30] ASTM C293/C293M-16, Standard Test Method for Flexural Strength of Concrete (Using Simple Beam With Center-Point Loading), ASTM International, West Conshohocken, PA, 2016, www.astm.org.

[31] ASTM C666/C666M–15, Standard Test Method for Resistance of Concrete to Rapid Freezing and Thawing, ASTM International, West 2015 Conshohocken, PA www.astm.org.

[32] N.K. Lee, S.Y. Abate, H. Kim, Use of recycled aggregates as internal curing agent for alkali-activated slag system, Constr. Build. Mater. 159 (2018) 286–296.

[33] D.P. Bentz, K.A. Snyder, Protected paste volume in concrete: extension to internal curing using saturated lightweight fine aggregate, Cem. Concr. Res. 29 (1999) 1863–1867.

[34] J.G. Guðmundsson, Long-term creep and shrinkage in concrete using porous aggregate –the effect of elastic modulus Master thesis, University of Reykjavík, Iceland, 2013.

[35] X. Ma, Z. Zhang, A. Wang, The transition of fly ash-based geopolymer gels into ordered structures and the effect on the compressive strength, Constr. Build. Mater. 104 (2016) 25–33.

[36] N. Li, C. Shi, Q. Wang, Z. Zhang, Z. Ou, Composition design and performance of alkali-activated cements, Mater. Struct. 50 (2017), doi:10.1617/s11527-017-1048-0.

[37] S.K. Nath, S. Maitra, S. Mukherjee, S. Kumar, Microstructural and morphological evolution of fly ash based geopolymers, Constr. Build. Mater. 111 (2016) 758–765.

[38] L. Alarcon-Ruiz, G. Platret, E. Massieu, A. Ehrlacher, The use of thermal analysis in assessing the effect of temperature on a cement paste, Cem. Concr. Res. 35 (2005) 609–613.

[39] F.U.A. Shaikh, S.W.M. Supit, Mechanical and durability properties of high volume fly ash (HVFA) concrete containing calcium carbonate (CaCO3) nanoparticles, Constr. Build. Mater. 70 (2014) 309–321.

[40] M. Mastali, A. Alzaza, S.K. Mohammad, P. Kinnunen, Z. Abdollahnejad, B. Woof, M. Illikainen, Using carbonated BOF slag aggregates in alkali-activated concretes, Materials 12 (8) (2019) 1288, doi:10.3390/ma12081288.

[41] M. Mastali, A. Dalvand, A.R. Sattarifard, Z. Abdollahnejad, M. Illikainen, Characterization and optimization of hardened properties of self-consolidating concrete incorporating recycled steel, industrial steel, polypropylene and hybrid fibres, Compos. Part B: Eng. 151 (2018) 186–200.

[42] S. Aydın, B. Baradan, The effect of fiber properties on high performance alkali-activated slag/silica fume mortars, Compos. Part B: Eng. 45 (2013) 63–69.

[43] A. Alzaza, M. Mastali, P. Kinnunen, L. Korat, Z. Abdollahnejad, V. Ducman, M. Illikainen, Production of lightweight alkali activated mortars using mineral wools, Materials 12 (10) (2019) 1695, doi:10.3390/ma12101695.

[44] T. Luukkonen, H. Sreenivasan, Z. Abdollahnejad, J. Yliniemi, A. Kantola, V. Telkki, P. Kinnunen, M. Illikainen, Influence of sodium silicate powder silica modulus for mechanical and chemical properties of dry-mix alkali-activated slag mortar, Constr. Build. Mater. Vol. 233 (2020,) 117354.

[45] Z. Abdollahnejad, M. Mastali, M. Falah, S. Mohammad, T. Luukkonen, M. Illikainen, Durability of the reinforced one-part alkali-activated slag mortars with different fibers, Waste and Biomass Valorization (2020) In press.

[46] G. Huseien, A.R.M. Sam, J. Mirza, M. Tahir, M.A. Asaad, M. Ismail, S. Wei, Waste ceramic powder incorporated alkali activated mortars exposed to elevated temperatures: performance evaluation, Constr. Build. Mater. 187 (2018) 307–317.

[47] L. Reig, M.M. Tashima, L. Soriano, M.V. Borrachero, J. Monzó, J. Payá, Alkaline activation of ceramic waste materials, Waste Biomass Valorization 4 (2013) 729–736.

[48] F. Pacheco-Torgal, J. Labrincha, C. Leonelli, A. Palomo, P. Chindaprasit, Handbook of alkali-activated cements, mortars and concretes, WoodHead Publishing Limited – Elsevier Science and Technology, Abington Hall, Cambridge, UK, 2014.

[49] A. Bhutta, M. Farooq, N. Banthia, Matrix hybridization using waste fuel ash and slag in alkali-activated composites and its influence on maturity of fiber-matrix bond, J. Cleaner Prod. 177 (2018) 857–867.

[50] X. Guo, X. Pan, Mechanical properties and mechanisms of fiber reinforced fly ash–steel slag based geopolymer mortar, Constr. Build. Mater. 179 (2018) 633–641.

[51] L. Deng, Y. Ma, J. Hu, S. Yin, X. Ouyang, J. Fu, A. Liu, Z. Zhang, Preparation and piezoresistive properties of carbon fiber-reinforced alkali-activated fly ash/slag mortar, Constr. Build. Mater. 222 (2019) 738–749.

[52] X. Guo, J. Yang, Intrinsic properties and micro-crack characteristics of ultra-high toughness fly ash/steel slag based geopolymer, Constr. Build. Mater. Vol. 230 (2020,) 116965.

[53] M.E. Gülşan, R. Alzeebaree, A.A. Rasheed, A. Niş, A.E. Kurtoğlu, Development of fly ash/slag based self-compacting geopolymer concrete using nano-silica and steel fiber, Constr. Build. Mater. 211 (2019) 271–283.

[54] N. Farhan, M. Sheikh, M. Hadi, Engineering properties of ambient cured alkali-activated fly ash-slag concrete reinforced with different types of steel fiber, J. Mater. Civ. Eng. 30 (2018) doi:10.1061/(ASCE)MT.1943-5533.0002333.

[55] H. El-Hassan, S. Elkholy, Performance evaluation and microstructure characterization of steel fiber-reinforced alkali-activated slag concrete incorporating fly ash, J. Mater. Civ. Eng. 31 (2019), doi:10.1061/(ASCE)MT.1943-5533.0002872.

[56] X. Gao, Alkali activated slag-fly ash binders: design, modeling and application Ph.D. Thesis, Eindhoven: Technische Universiteit Eindhoven, The Netherlands, 2017.

[57] H. Funke, S. Gelbrich, L. Kroll, The durability and performance of short fibers for a newly developed alkali-activated binder, Fibers 4 (2016), doi:10.3390/fib4010011.

[58] Y. Alrefaei, J. Dai, Tensile behavior and microstructure of hybrid fiber ambient cured one-part engineered geopolymer composites, Constr. Build. Mater. 184 (2018) 419–431.